THESIS FOR THE DEGREE OF LICENTIATE OF PHILOSOPHY

Empirical Modeling of Solar Induced Variations of Nitric Oxide in the Upper Mesosphere and Lower Thermosphere

JOONAS KIVIRANTA

CHALMERS
UNIVERSITY OF TECHNOLOGY

Department of Space, Earth and Environment
Division of Microwave and Optical Remote Sensing
Chalmers University of Technology
Gothenburg, Sweden 2018

Empirical Modeling of Solar Induced Variations of Nitric Oxide in the Upper Mesosphere and Lower Thermosphere
JOONAS KIVIRANTA

Department of Space, Earth and Environment
Division of Microwave and Optical Remote Sensing
Chalmers University of Technology
SE-412 96 Gothenburg

Typeset in LaTeX
Gothenburg, Sweden 2018

Empirical Modeling of Solar Induced Variations of Nitric Oxide in the Upper Mesosphere and Lower Thermosphere
JOONAS KIVIRANTA
Department of Space, Earth and Environment
Chalmers University of Technology

Abstract

Nitric Oxide (NO) is produced by solar photolysis and auroral activity in the upper mesosphere and lower thermosphere region and can, via transport processes, eventually impact the ozone layer in the stratosphere. This thesis uses measurements of NO taken between 2004 and 2016 by the Odin Sub Millimetre Radiometer (SMR) to build an empirical model which links the prevailing solar and auroral conditions with the measured number density of NO. The measurement data are averaged daily and sorted into altitude and magnetic latitude bins. For each bin, a multivariate linear fit with five inputs, the planetary K-index, solar declination, and the F10.7cm flux, and two newly devised indices which take the planetary K-index and the solar declination as inputs in order to take NO created on previous days into account, constitutes the link between environmental conditions and measured NO. This results in a new empirical model, SANOMA, which only requires the previously mentioned indices to estimate NO between 85 km-115 km and 80° S-80° N in magnetic latitude. Furthermore, this work compares the NO calculated with SANOMA and an older model, NOEM, with measurements of the original SMR-dataset, as well as measurements from four other instruments: ACE, MIPAS, SCIAMACHY, and SOFIE. The results suggest that SANOMA can capture roughly 31-70% of the variance of the measured datasets near the magnetic poles, and between 16-73% near the magnetic equator. The corresponding values for NOEM are 12-38% and 7-40%, indicating that SANOMA captures more of the variance of the measured datasets than NOEM. The simulated NO for the entire latitude range was on average 20% larger for SANOMA, and 78% larger for NOEM, than the measured NO. Two main reasons for SANOMA outperforming NOEM are identified. Firstly, the input data (Odin SMR NO) for SANOMA spans over 12 years covering more than one solar cycle, while the input data for NOEM from the Student Nitric Oxide Experiment (SNOE) only covers two years (1998-2000). Additionally, some of the improvement can be accredited to the introduction of the two new indices, since they include information of auroral activity on prior days which can significantly enhance the number density of NO in the MLT during winter in the absence of sunlight. As a next step, SANOMA could be used as input in chemical climate models, as apriori information for the retrieval of NO from measurements, or as a tool to compare Odin SMR NO with other instruments.

Keywords: nitric oxide, empirical modeling, Odin, SANOMA, mesosphere, thermosphere.

Acknowledgements

I would like to thank my supervisors Donal Murtagh, Patrick Eriksson, and Kristell Pérot for helping throughout the process of the licentiate, as well as my colleagues for general support and many great coffee room discussions. Joonas Kiviranta,

Gothenburg, May 2018

Contents

1
Introduction

How much of the observed climate change can be attributed to a solar source? This is the fundamental question that many scientists have attempted to answer, with no definitive answer. In general, it seems that subsequent to the first half of the 20th century, solar influence has played a minor role in the observed increase of mean surface temperatures (Gray et al., 2010). Nonetheless, investigating the solar influence on climate remains of high interest since it can affect the climate in other ways, such as the regional climate variability. In an effort to quantify possible effects, the World Climate Research Program (WCRP) initiated the Coupled Model Intercomparison Project (CMIP) (Eyring et al., 2016). This project requires knowledge on a multitude of atmospheric constituents in order to accurately model possible solar effects. Among them, is Nitric Oxide (NO). NO is a reactive free radical, and together with Nitrogen dioxide (NO_2), constitutes the NO_x compounds. Whereas tropospheric NO_x may originate from both natural sources, such as forest fires, and anthropogenic sources, such as combustion engines (Wallace and Hobbs, 2006), NO in the mesosphere and lower thermosphere (MLT, ∼50-150 km) has a purely natural origin.

Knowledge about NO in this region is of great importance, because it can affect the temperature of the layers below and destroy stratospheric ozone. In the MLT, NO can be produced by two mechanisms: either direct radiation from the sun in the form of solar-soft x-rays ($8 \leq \lambda \leq 12$ Å) or energetic particle precipitation (EPP) (Barth et al., 1999; Sinnhuber et al., 2012). These particles can include electrons, protons, or heavier ions. These may originate directly from the sun, from aurorae and the radiation belts during geomagnetic storms, or from outside of the solar system. Previous studies have established that EPP from geomagnetic activity dominates the variation of NO near the magnetic poles, while solar-soft x-rays contribute more near the magnetic equator (Gérard and Barth, 1977; Barth et al., 1999; Sinnhuber et al., 2012).

Over the past several decades, at least six satellites have measured NO in the MLT region. This thesis focuses on measurements from the currently active Odin SMR (Sub Millimetre Radiometer). The limitation of satellite measurements is that they only cover certain locations and periods of time. Yet, many applications, such as chemical models of the upper atmosphere, require information on the amount of NO at any given time or location. To help bridge this gap, a model which connects known environmental conditions, such as geomagnetic activity, with measured NO can help to provide an estimate of NO at any time and place. Such a model can also help validate and constrain poorly resolved or underdetermined parameters of first principle models.

This study focuses on the natural variability of NO in the MLT. We aim to create an empirical model based on 12 years of Odin SMR NO measurements to link prevailing solar and geomagnetic conditions with the measured NO. This model could then be used in the applications mentioned in the paragraph above, to help quantify the solar influence on our climate.
The introduction to this thesis presents the pertinent theory to understand the resulting Paper A. Chapter 2 starts by introducing the vertical structure of the atmosphere, followed by NO chemistry and dynamics in the MLT, and is concluded with a description of geomagnetic and solar activity relevant to the upper mesosphere and lower thermosphere. Chapter 3 describes Odin SMR and elaborates on the process which transforms raw measurements to the NO data product. Additionally, it offers an overview of satellite measurements of NO from other satellites as well, and briefly compares the various datasets. Finally Chapter 4 summarizes the paper which results from this research and provides an outlook for future work.

2

NO in the Middle Atmosphere

This Section introduces the key concepts which govern the creation and destruction of NO in the atmosphere with the main focus on the upper mesosphere and lower thermosphere. It also presents pertinent information on the Earth's magnetic field, since it influences the geographic location at which nitric oxide is created. All of this theory will be necessary to understand and interpret satellite measurements of NO processed in Paper A.

The atmosphere is the layer of gas that surrounds the Earth. By volume, its three largest constituents are Nitrogen (78.08%), Oxygen (20.95%), and Argon (0.93%). Additionally, the atmosphere contains smaller amount of other trace gases, such as water vapor, carbon dioxide, or nitrous oxide (Wallace and Hobbs, 2006). The average density of the atmosphere at sea level is 1.25kg/m^3, decreasing with higher altitude. Atmospheric pressure roughly follows the relationship

$$p \simeq p_0 e^{-z/H}, \tag{2.1}$$

in which p is the pressure, p_0 is the pressure at sea level, z is the altitude above sea level, and H is the scale height, which is the distance over which the pressure decreases by a factor of Euler's number e. In the lowest 100 km of the atmosphere, the scale height ranges from 7 to 8 km. This region of the atmosphere is known as the homosphere. Within the homosphere, the atmospheric gases are thought to be well mixed due to turbulent processes, meaning that their relative concentrations are the same regardless of location. At roughly 100 km lies the turbopause above which turbulent processes no longer mix the air. This results in a region called the heterosphere, in which the individual constituent gases gradually become stratified such that the compounds with the highest molecular weight lay at the bottom. Beyond the division into the homo- and heterosphere, Figure 2.1 illustrates how the temperature of the atmosphere can be used to further categorize it into various layers. The mesosphere and thermosphere constitute the regions of interest in this work. In the mesosphere, the temperature of the atmosphere decreases until we reach the mesopause at roughly 80 km. Above this altitude, molecular nitrogen and oxygen absorb sufficient amounts of solar radiation to result in an increase in temperature. The combination of the upper Mesosphere and Lower Thermosphere is referred to as the MLT region. The following two sections elaborate on the dynamics and chemistry of this region.

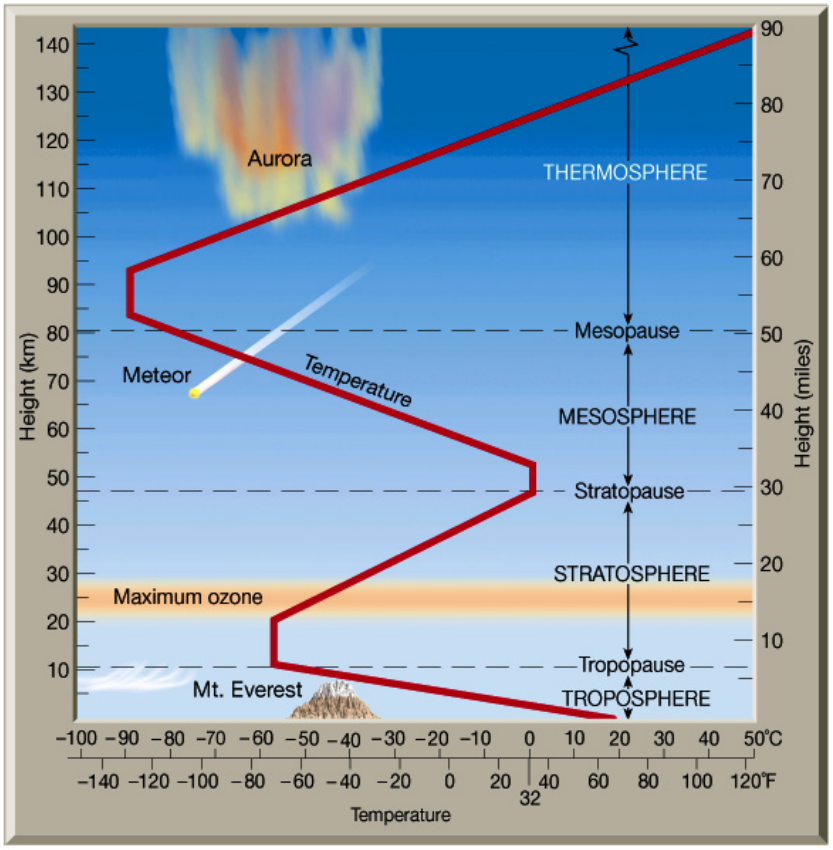

Figure 2.1: The vertical structure of the atmosphere (Lutgens et al., 2001).

2.1 Nitric Oxide Chemistry in the Upper Mesosphere and the Lower Thermosphere

Two mechanisms can create NO in the MLT: either direct solar radiation from the sun in the form of solar-soft x-rays ($8 \leq \lambda \leq 12$ Å) or energetic particle precipitation (EPP) (Barth et al., 1999; Sinnhuber et al., 2012). EPP refers to the processes of interaction between the atmosphere and incoming highly energetic particles, which can include protons, electrons, or heavier ions. These may originate directly from the sun, from aurorae and the radiation belts during geomagnetic storms, or from outside of the solar system.

Previous studies have established that EPP from geomagnetic activity dominates the variation of NO near the magnetic poles, while solar-soft x-rays contribute more near the magnetic equator (Gérard and Barth, 1977; Barth et al., 1999; Sinnhuber et al., 2012). NO in the MLT is created through the reaction between molecular oxygen and an excited nitrogen according to the equation

$$N(^2D) + O_2 \rightarrow NO + O, \tag{2.2}$$

in which N(^{2}D) denotes an excited nitrogen atom. Excited nitrogen is created by the two reactions

$$N_2 + e^* \rightarrow N(^2D) + N, \tag{2.3}$$

and

$$NO^+ + e \rightarrow N(^2D) + O, \tag{2.4}$$

in which e* indicates an energetic electron, originating from either EPP or from the interaction of solar soft x-rays with the atmospheric gases (Marsh et al., 2004). This implies that geomagnetic or solar activity is necessary to form NO in the presence of an oxygen molecule. On the other hand, solar light destroys NO in the cannibalistic reaction

$$NO + hv \rightarrow N + O, \tag{2.5}$$

$$N + NO \rightarrow N_2 + O. \tag{2.6}$$

Therefore the amount of NO is affected by seasonal variation of sunlight. Under sunlit conditions in the MLT region, NO has a chemical lifetime of less than one day, whereas during the polar night in winter, it may persist for several weeks (Minschwaner and Siskind, 1993). Hence, variations in the amount of NO may be induced by either changes in solar or geomagnetic activity, as well as season. Variations in solar activity can follow a period of 27-days, or long-term fluctuation with the 11-year solar cycle(Barth et al., 1988).

2.2 Dynamics in the Upper Mesosphere and the Lower Thermosphere

So far we have established basic equations which describe the creation and destruction of NO in the MLT. To add to the complexity of the atmospheric system, this section introduces some key concepts in dynamics in the MLT region which can cause additional variation in NO: diurnal variation and associated tidal effects, or mean meridional circulation.

Model calculations of the production and dissociation rates of NO in the MLT by Strobel (1971) suggested that NO number density at 06:00 local time could be roughly 20% higher than at 18:00 local time at an altitude of 110 km. Lower down between 70 and 105 km Marsh and Russell (2000) argued that downward tidal velocities coincided with observed increases is NO. Close to the equator at an altitude of 85 km, the tidal effect could enhance NO VMR by up to 80% by transporting NO created at higher altitudes downwards, with a lesser effect close to the poles.

The polar vortex, which is a feature of the mean meridional circulation, constitutes another important concept in the dynamics of the atmosphere in the MLT. It is a stable wind system which forms around the poles during winter and reduces or prevents the mixing of polar, and mid-latitude air (Schoeberl et al., 1992). As a consequence, NO-rich mesospheric air can descend from the MLT into the lower mesosphere and stratosphere (Fisher et al., 1993) and eventually partake in catalytic cycles which contribute to the destruction of stratospheric ozone (Konopka et al., 2007). Figure 2.2 illustrates the polar vortex system. The phenomenon when EPP

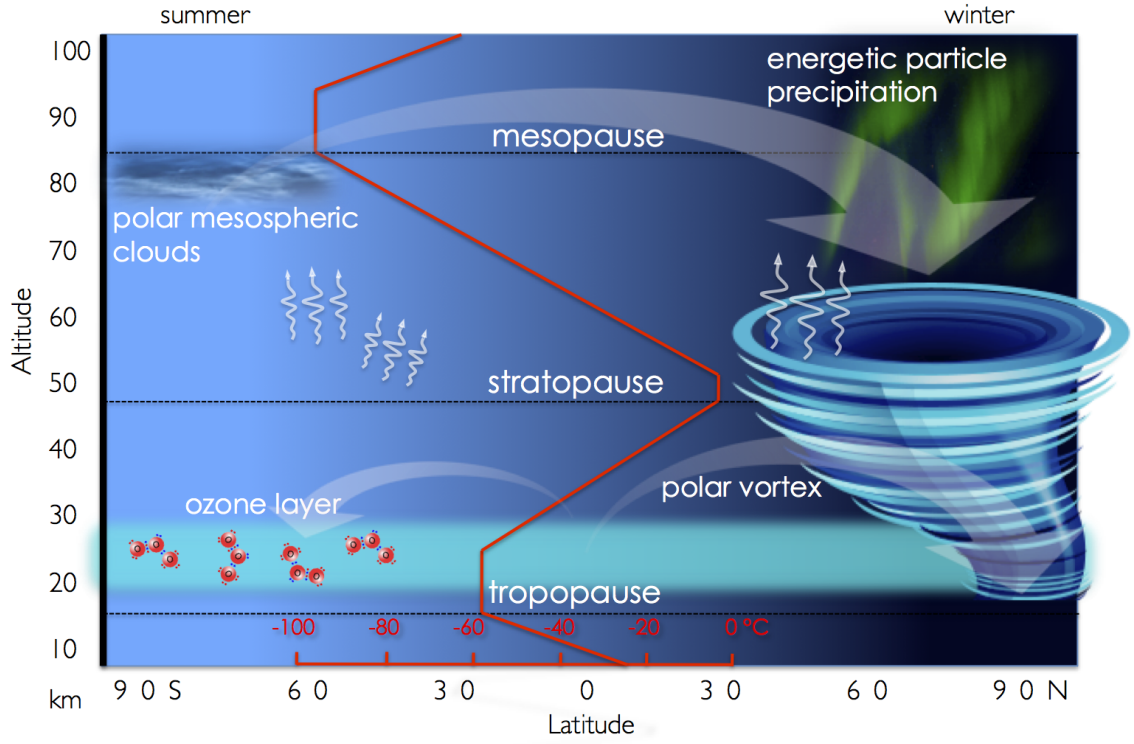

Figure 2.2: A schematic of the polar vortex and energetic particle precipitation. (University of Colorado Boulder).

creates NO in the MLT region, subsequent to which this NO-rich air descends into the stratosphere is called the EPP indirect effect (Sinnhuber et al., 2012). The descent can be further enhanced during SSW events (Pérot et al., 2014). SSW is the event in which the atmosphere rapidly warms at the 10hPa pressure level, with a rate of up to 70K/week, following a perturbation of the polar vortex (Labitzke and Kunze, 2009). This event is often followed by the reformation of an upper stratospheric vortex associated with an elevated stratopause, which can bring more NO down into the lower layers of the atmosphere.

2.3 Geomagnetic and Solar Activity

To further complicate matters, the Earth's magnetic field dictates the locations at which charged particles enter the Earth's atmosphere. Hence, understanding the properties and the change in the magnetic field constitutes an additional dimension to knowledge on NO in the MLT. Elsasser (1939) proposed that the existence of the Earth's magnetic field could be traced to motions of the metallic interior of the Earth. The 12th International Geomagnetic Reference Field (IGRF) contains the newest mathematical models describing the large-scale internal part of the Earth's magnetic field between epochs 1900 A.D. and present (Thebault et al., 2015). Two relevant observations for EPP are that the Earth's magnetic field is neither symmetric nor static. Figure 2.3 depicts the change in the locations of the magnetic north and south poles over time. The red and blue dots illustrate the locations of the magnetic and

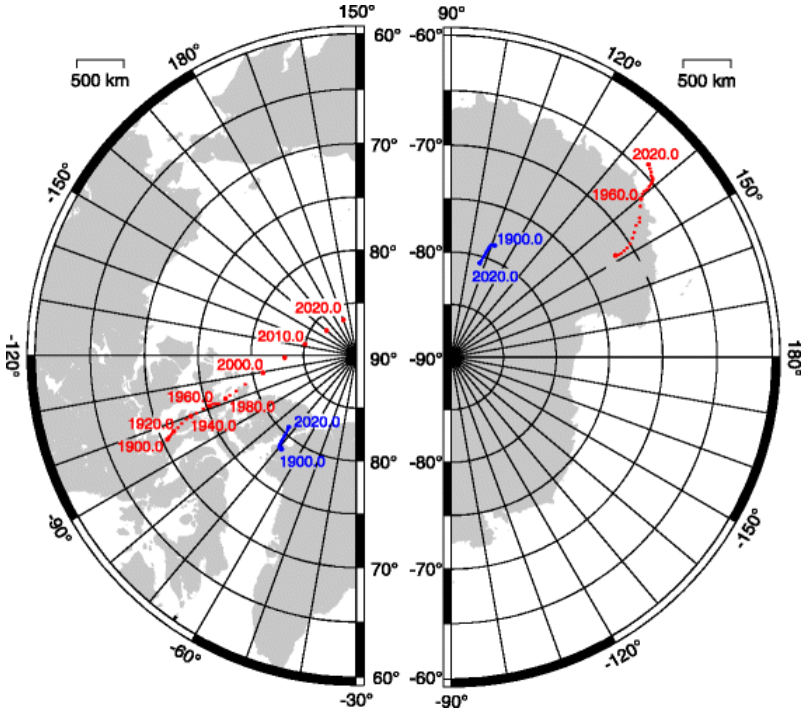

Figure 2.3: Geographic locations of the magnetic (in red) and geomagnetic (in blue) poles over time. (Thebault et al., 2015).

geomagnetic poles, respectively. The geomagnetic poles are the locations of the poles in a dipole approximation of the magnetic field, while the magnetic poles are defined as the locations at which a freely rotating needle of a compass would point straight down. Interestingly, while the southern magnetic pole has moved roughly 5° north during the past 100 years, its northern counterpart has traversed 5° between 2000 and 2010, continuing with a velocity of roughly 50 km/year on a traverse towards Siberia. Compared to the geographical pole, the southern and northern magnetic poles are currently offset by some 25° and 5°, respectively.

Incoming EPP can excite oxygen which upon de-excitation emits visible light. This phenomenon creates the aurorae, typically in green or red. As demonstrated by Figure 2.4, the aurorae can be seen in ovals centered around 10°-20° from the magnetic poles. NO can essentially be viewed as a by-product of this very same process. Hence, some of the NO in the MLT will be produced in the auroral oval (Solomon et al., 1999). Furthermore, Figure 2.4 suggests that the auroral oval is more offset in the southern than in the northern hemisphere, as a consequence of the locations of the magnetic poles. For comparing NO measurements at various, this offset gives rise to the need of a coordinate system which is based on geomagnetic latitude instead of geographic latitude. An altitude-corrected geomagnetic latitude can be calculated with the 12th IGRF model Thebault et al. (2015), resulting in coordinates such as in Figure 2.5. Rather annoyingly from a European perspective, the auroral zone above Europe is further up north than in North America, meaning that we have to travel further up north to see the northern lights.

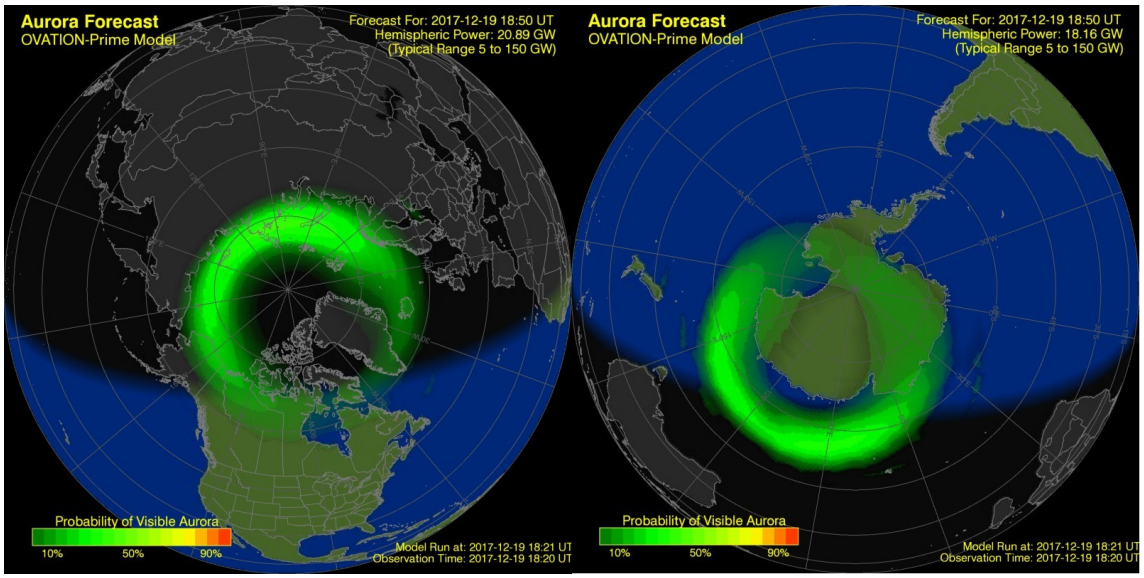

Figure 2.4: Auroral ovals in the northern and southern hemispheres. These correspond to the locations at which auroral activity produces NO (NOAA, a,b).

2.3.1 Proxies for Geomagnetic and Solar Activity

Measurements of the irregular variations of the horizontal component of the Earth's magnetic field constitute a geomagnetic activity index, the Kp-index (Menvielle and Berthelier, 1991). It ranges from 0-9 on a quasi-logarithmic scale with higher values corresponding to higher activity. It is derived every 3 hours from a network of measurements stations located between $\sim$40° N-60° N as well as at $\sim$40° S geographical latitude. A similar index, the Ap-index is exponentially proportional to the Kp-index. Finally, the Ae-index is another measure for geomagnetic activity and has been suggested to correlate more directly with NO in the MLT region than the Kp- or Ap-index (Hendrickx et al., 2015). The Ae-index derives from measurement stations closer to the magnetic poles than the Kp-index (Menvielle et al., 2011). The Kp- and Ap-indices for this study are obtained from the National Oceanic and Atmospheric Administration (NOAA) whereas the Ae-index originates from http://wdc.kugi.kyoto-u.ac.jp/aedir/.
To describe solar activity, the 10.7 cm solar radio flux is among the most widely used indices. It constitutes a proxy for the incoming solar soft x-rays and is based on the solar radio emission in a 100 MHz-wide band centered around 2800 MHz (Tapping and Detracey, 1990). This study uses the observed daily mean 10.7 cm from the NOAA. The total radiation flux centered around the Lyman-α line defines an alternative proxy for solar activity and originates from http://lasp.colorado.edu/lisird/data.html. Figure 2.6 shows the F10.7cm flux over time. Over the measurement period of Odin SMR, solar activity decreased until 2009, subsequent to which it rose to reach a maximum in 2014, followed by another decline. In the context of this work, the solar cycle is integral to understanding radiation-related variations of NO.

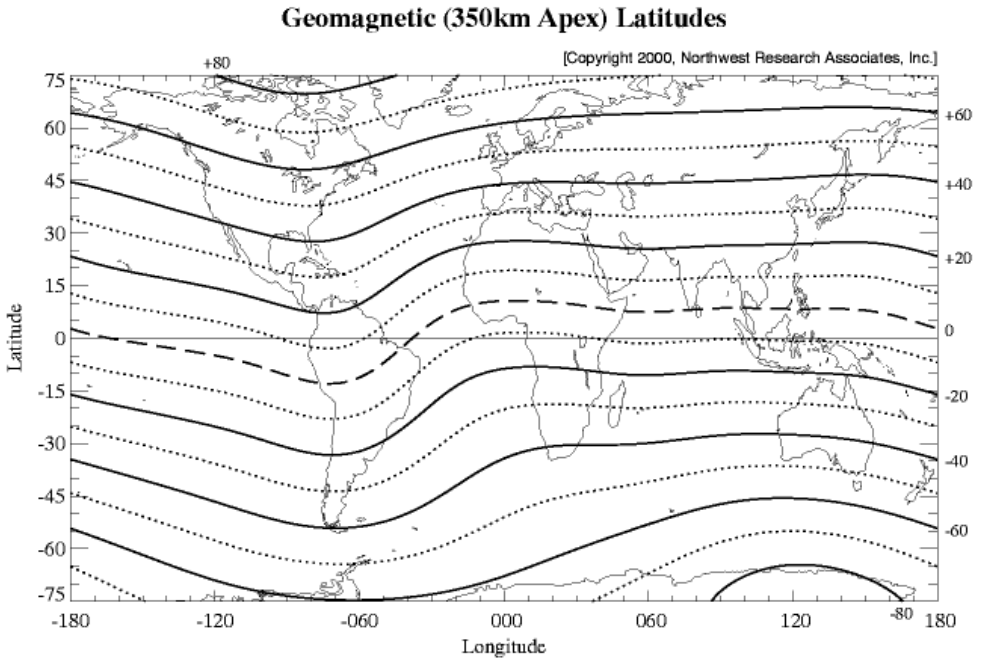

Figure 2.5: Geomagnetic latitude (NWRA).

Figure 2.6: F10.7cm flux over time. (NOAA)

3

Satellite Measurements of Nitric Oxide in the Upper Atmosphere

This chapter describes the NO measurements of Odin SMR in detail. First, Section 3.1 desribes the Odin satellite, SMR, and the required steps between the raw measurement and the NO product. For a general overview and comparison, Section 3.2 describes other satellites which measure NO in the MLT region.

3.1 Odin SMR Nitric Oxide

Odin is a satellite built in co-operation between Sweden, Canada, France, and Finland. It was launched in February 2001 and carries two instruments: the Optical Spectrograph and InfraRed Imager System (OSIRIS) and the Sub-Millimetre Radiometer (SMR) (Murtagh et al., 2002). Its name stems from Norse mythology in which Odin is associated with a myriad of attributes, including poetry, sorcery, and war. Odin was no simple brute since according to the saga he sacrificed one of his eyes in order to gain permission to drink from the well of wisdom (McCoy, 2017). The author of this work has acquired information from sources close to the Odin satellite, that the satellite was called Odin because its most notable feature includes one eye-like large antenna, much like the mythological god Odin. Sources close to the Odin satellite have also told the author that the instruments on board the satellite were originally supposed be called Huginn and Muninn, two raven sitting on Odin's shoulders. On his quest towards wisdom, Odin used Huginn and Muninn, which would fly out and relay information on the affairs of the world to him, but unfortunately these names were already reserved for another science project. Hence, the two instruments were named the OSIRIS and SMR.
In addition to many other species such as ozone and carbon monoxide, Odin SMR has been observing NO thermal emission lines in a band centered around 551.7 GHz since 2004 (Sheese et al., 2013). During the first years of operation, Odin split its observation time between aeronomy and astronomy observation, but subsequent to 2007 it has dedicated all of its time to aeronomy. The mode in which Odin measures NO was operated one 24-hour period per month prior to 2007. Subsequent to 2007, Odin measures NO four 24-hour periods each month. Odin follows a sun-synchronous orbit with ascending and descending nodes around 06:00 and 18:00 local time, respectively, and provides near-global coverage between approximately 82°S and 82°N (Nordh et al., 2003). Since Odin measures thermal emission, the resulting data includes both day-time and night-time measurements. The frequency

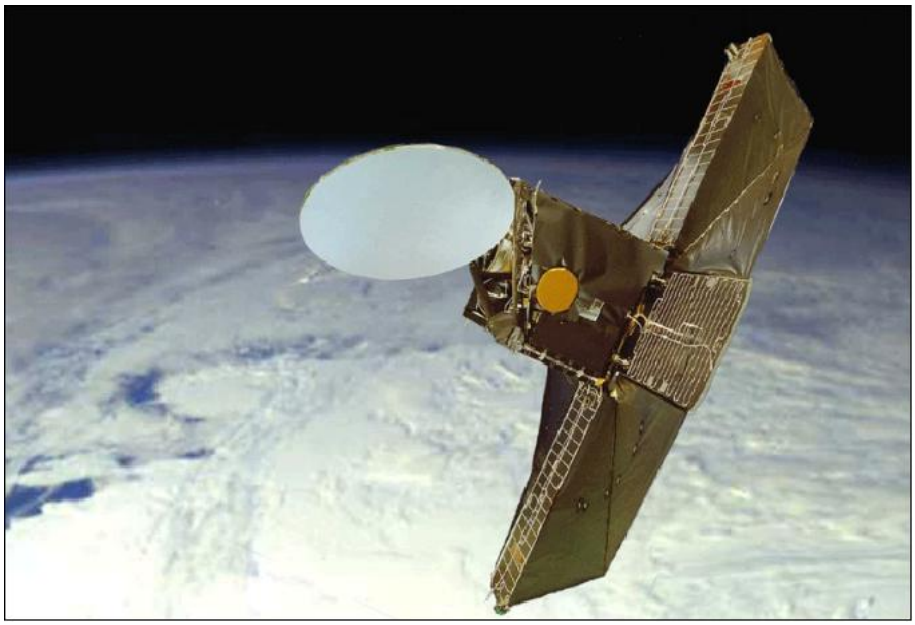

Figure 3.1: The satellite Odin (credit Svenska Rymdaktiebolag SSC).

range of the measured spectrum runs from 551.15 to 552.15 GHz contains strong ozone emission lines at 551.45 and 552.05 GHz, as well as weaker NO emission lines at 551.2 and 551.55 GHz (Eriksson, 1999).

Odin scans the limb of the atmosphere and measures emission spectra at various tangent altitudes. The tangent altitude H_0 is defined as shown in Figure 3.2. One "scan" of the instrument contains individual measurements from various altitudes. Figure 3.3 illustrates the measured brightness temperature, T_b in Kelvin, as a function of Frequency. The various lines correspond to tangent altitudes as indicated by the legend. The lower the tangent altitude, the higher the baseline of the measured radiation is. This is due to radiation from species such as water vapor. The measured spectrum can become saturated at the lower frequencies, meaning that the brightness temperature is nearly constant within the given frequency range. The ozone emission peaks are clearly visible around 551.45 and 552.05 GHz at the lower altitudes. The NO emission lines become faintly visible in the mesospheric and thermospheric altitudes. The lower panel of 3.3 depicts the average spectrum from the MLT region in which faint peaks at the NO emission frequencies of 551.2 and 551.55 GHz can be seen rising above the measurement noise level.

Inferring the amount of NO as a function of altitude from a set of measured spectra as depicted in Figure 3.3 constitutes an inverse problem. Figure 3.4 attempts to clarify the difference between a forward, and an inverse problem. In our case, the atmospheric state is the VMR of NO as a function of altitude, and the output is the measured spectrum. If we were to know the state, and would feed this state into a model to calculate the output, we would have a forward problem. This could be readily solved with a radiative transfer model, such as the Atmospheric Radiative Transfer Simulator (ARTS) (Eriksson et al., 2011). The inverse problem is more difficult, since an infinite combination of various amounts of NO as a function of altitude could result in the measured spectrum. Since there is no unique solution,

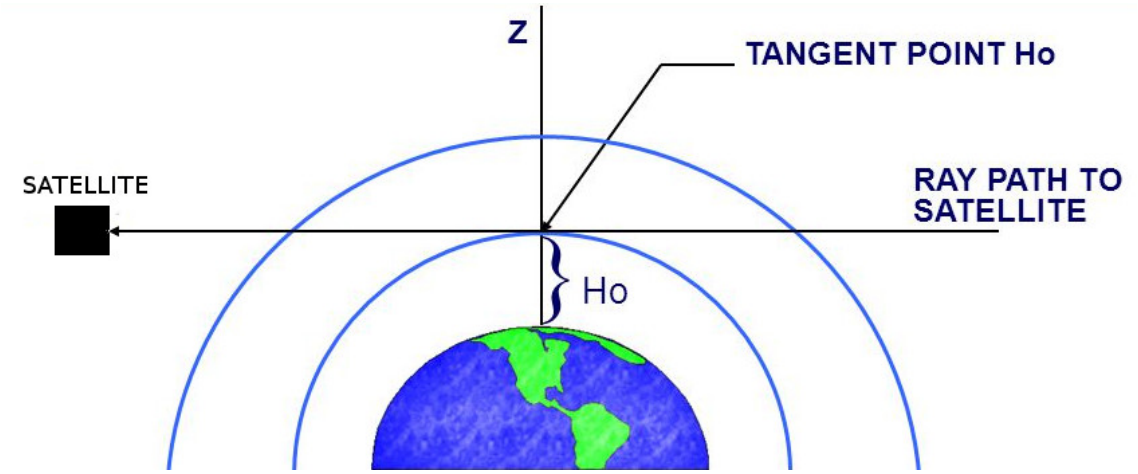

Figure 3.2: The observation geometry of a limb-sounding satellite, such as Odin (adapted from (SABER)).

the problem is said to be ill-posed. To solve the problem, we must use an inversion algorithm. Figure 3.5 illustrates the approach.
To infer the atmospheric state, we can use an Optimal Estimation Method (OEM) (Rodgers, 1976; Urban et al., 2005) together with statistical knowledge on the expected profile of NO VMR for the given measurement time and location (e.g. Siskind et al. (1998)). This statistical knowledge is also known as the apriori, and constrains the problem such that the OEM can converge on a solution through iteration. The result of the inversion algorithm on the measured spectrum in Figure 3.3 can be seen in Figure 3.6. The green and blue lines depict the apriori, and retrieved NO profiles, respectively. The vertical resolution of the NO profile varies around 5 km, depending on the altitude and the individual scan. The horizontal error bars on the retrieved NO reflect an estimated error of one standard deviation for the measurement at each altitude. Contributors to this estimate include uncertainties in the pointing of the satellite, the calibration of the brightness temperature measurements, or the information on the location and intensity of the emission lines within the measured frequency range, to name a few. As a final step, the acquired NO VMR profile can be converted into number density, expressed in molecules of NO per cm^3. For this conversion we apply the ideal gas law in which the pressure and temperature originate from an apriori background atmosphere. The newest version of Odin SMR NO carries the name V3.0 and its validation is ongoing. The following Section will elaborate on the validation of NO in the MLT region.

3.2 An Overview of Nitric Oxide Measurements in the Upper Atmosphere

Among the first NO measuring satellites were the Solar Mesosphere Explorer (SME) (Barth, 1992), and the Student Nitric Oxide Experiment (SNOE) (Solomon et al., 1999), which operated between 1981-1989 and 1998-2000, respectively. A new generation of satellites, including Odin, has provided longer datasets for more advanced

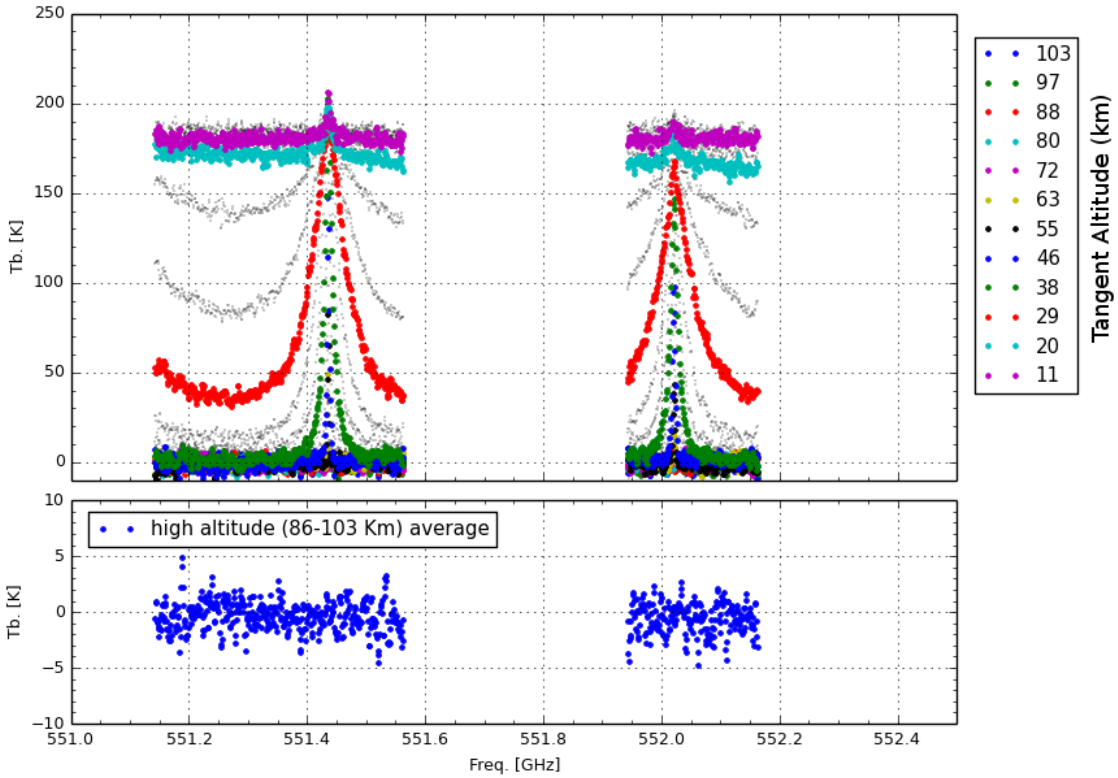

Figure 3.3: An example of measured emission spectra from one scan and the mean spectrum between 86 and 103 km, frequency mode 21.

Table 3.1: Overview of the various NO datasets.

Instrument	Period	Latitudes	Altitudes (km)	Technique	Wavelength
SMR	2004-	82°S - 82°N	85-115	Microwave Emission	544 μm
SOFIE	2007-	80°S - 60°S, 60°N - 80°N	40-140	Solar Occultation	5.316 μm
SCIAMACHY	2008-2012	88.75°S - 88.75°N	60-160	UV Scattering	230-314 nm
ACE	2004-	82°S - 82°N	70-110	Solar Occultation	5.18-5.43 μm
MIPAS	2005-2012	82°S - 82°N	70-120	Infrared emission	5.3 μm

studies. Table 3.1 lists five NO-measuring satellites with some key information. Apart from Odin, the Solar Occultation For Ice Experiment (SOFIE) (Gordley et al., 2009) , SCanning Imaging Absorption SpectroMeter for Atmospheric CHartographY (SCIAMACHY) (Bender et al., 2013), the Atmospheric Chemistry Experiment (ACE) (Bernath et al., 2005), and the Michelson Interferometer for Passive Atmospheric Sounding (MIPAS) (Fischer et al., 2008) constitute some past and current MLT NO measuring instruments. Table 3.1 lists their underlying principles and measurement regions.

Due the respective measurement techniques listed in 3.1, SMR and MIPAS measure day- and night-time NO, while SCIAMACHY only includes day-time NO. SOFIE and ACE NO originates from sunrise or sunset due to the solar occultation technique. Direct comparison of the various satellites is difficult, since NO varies on a very short time-scale in the MLT region including diurnal and tidal variations. Bender et al. (2015) included day-time measurements to calculate daily zonal average NO from SMR, SOFIE, SCIAMACHY, and ACE, in order to enable an indirect comparison

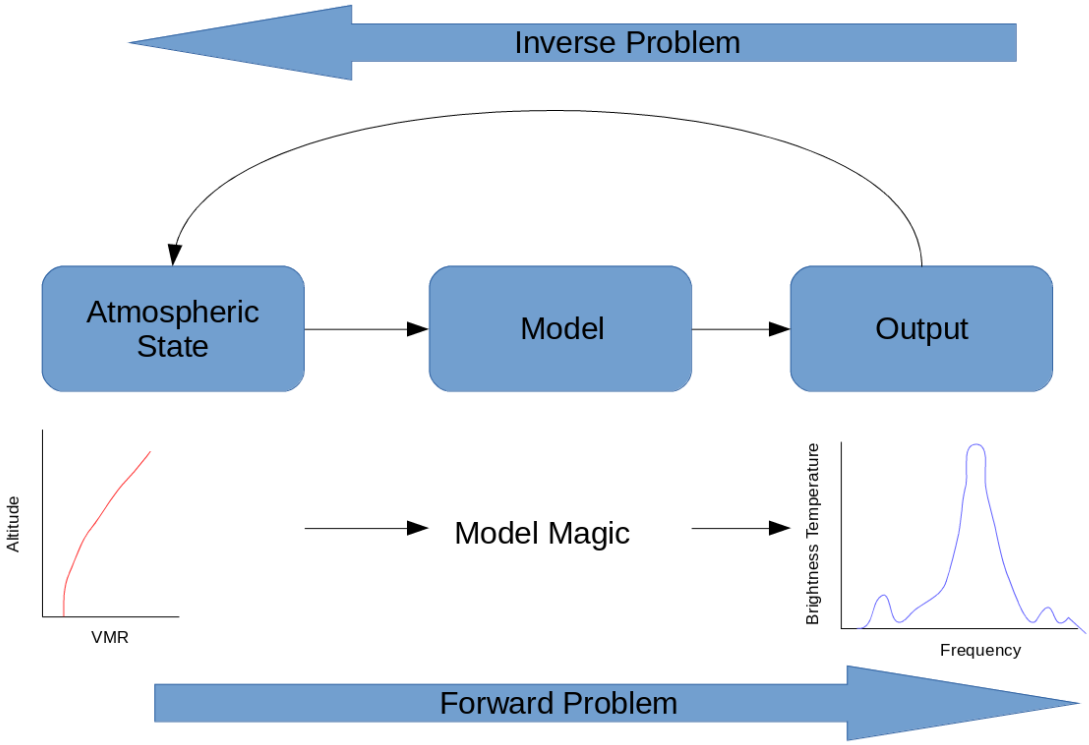

Figure 3.4: The difference between a forward and an inverse model.

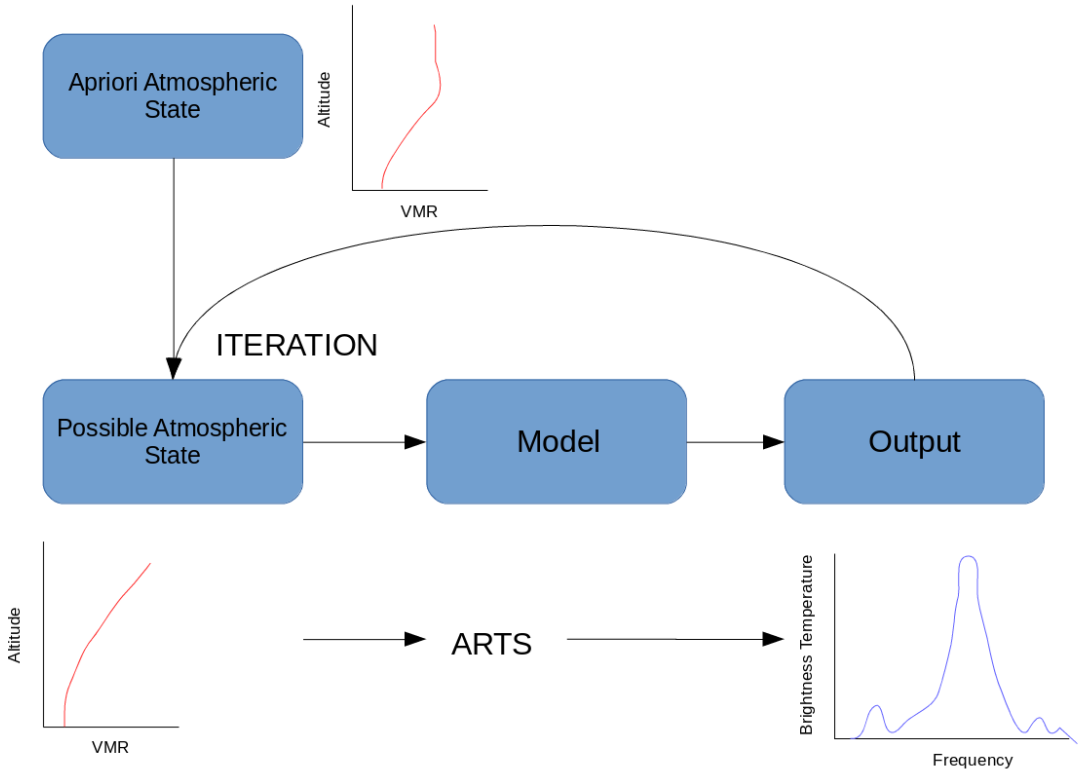

Figure 3.5: Solving the inverse problem.

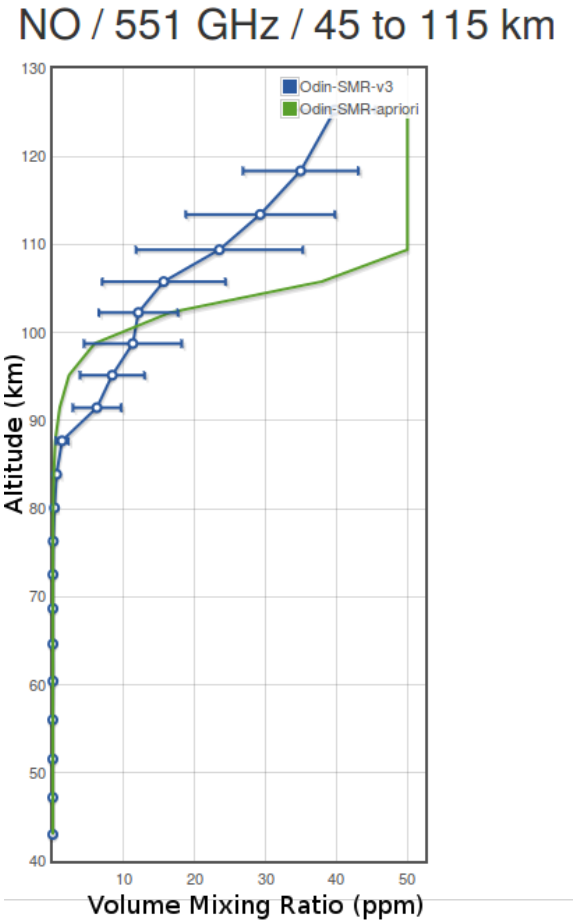

Figure 3.6: An example of retrieved and apriori NO profiles from the spectra in 3.3.

of their results. They found that despite the various measurement techniques, the NO number densities agree well and lie within the chosen statistical error bars (95% confidence interval). Furthermore, Bender et al. (2015) attribute remaining differences to the various MLT measurement schedules and the latitude-time coverage of the instruments. For instance, SCIAMACHY only provides day-time measurements, resulting in a low bias compared to the other instruments, since sunlight dissociates NO in the MLT region. In general, validating these NO measurements offers a challenge, since there are neither in-situ measurements, nor frequent coinciding measurements between satellites for comparison.

4

Summary of the Paper and Future Work

4.1 Summary of Paper I

This study proposes a new empirical model for the calculation of Nitric Oxide (NO) in the upper mesosphere and lower thermosphere (MLT). The work was inspired by an empirical model of NO in the MLT region called the Nitric Oxide Empirical Model (NOEM), in which Marsh et al. (2004) use measurements from the Student Nitric Oxide Experiment (SNOE) satellite, which operated between 1998 and 2000, to create a model which simulates the number density (molecules/cm^3) of NO as a function of altitude and magnetic latitude. For this, NOEM only needs three inputs: the Kp-index, the solar declination, and the F10.7cm flux. These three indices can be seen as proxies to describe the geomagnetic, seasonal, and solar radiation induced variations of NO, respectively. The design of the model was based on Empirical Orthogonal Function (EOF) analysis and can deliver NO number density between 100 and 150 km in altitude, and -82.5° and 82.5° in geomagnetic latitude.

In this study, we create a similar model, called the SMR Acquired Nitric Oxide Model Atmosphere (SANOMA) but with three key differences. Firstly, we use NO measurements from Odin SMR which span a period of over 12 years between 2004 and 2016, covering over one solar cycle. We demonstrate, that using this longer data series, the resulting empirical model will be more accurate since the Odin SMR measurement period contains a wider range of environmental conditions which lead to various amounts of NO. Secondly, we introduce two additional indices which attempt to account for NO accumulated on previous days during polar night. These two indices only require the Kp-index and solar declination as inputs. The resulting model hence needs the same three inputs as NOEM. Finally, we use multivariate linear fits to find a function which links the three inputs to the measured zonally averaged daily mean NO from Odin SMR.

SANOMA can provide estimates of NO number density between 85 km-115 km in altitude, and -80° and 80° in geomagnetic latitude. This study evaluates SANOMA by comparing its output to the original SMR measurements. SANOMA can explain some 64% of the variance of the NO of SMR NO. The average NO number density differs only by 0.1% between the model and measurements.

Furthermore, this work compares SANOMA and NOEM, with NO from SMR and four other instruments: ACE, MIPAS, SCIAMACHY, and SOFIE. The results suggest that SANOMA can capture roughly 31-70% of the variance of the measured

datasets near the magnetic poles, and between 16-73% near the magnetic equator. The corresponding values for NOEM are 12-38% and 7-40%, indicating that SANOMA captures significantly more of the variance of the measured datasets than NOEM. The simulated NO for these regions was on average 20% larger for SANOMA, and 78% larger for NOEM, than the measured NO. Two main reasons for SANOMA outperforming NOEM can be identified. Firstly, the input data (Odin SMR NO) for SANOMA spans over 12 years, while the input data for NOEM from the Student Nitric Oxide Experiment (SNOE) only covers 1998-2000, a period of low solar activity. Additionally, some of the improvement can be accredited to the introduction of the two new indices, since they include information of geomagnetic activity on prior days which can significantly enhance the number density of NO in the MLT during winter in the absence of sunlight.

4.2 Outlook

As a continuation of this thesis, the work presented in Paper A could be expanded upon by utilizing SANOMA in various applications. These may include using SANOMA NO as direct input in chemical models of the atmosphere, such as the Whole Atmosphere Community Climate Model (WACCM) (Smith et al., 2014), or as a priori information for satellite retrievals. Moreover, SANOMA could be used as a tool to compare SMR NO with other datasets. Alternatively, SANOMA could act as a transfer function for NO measurements.
Beyond the context of SANOMA, the newest V3.0 NO should be validated prior to expanded use. Since SMR comprises of measurements from a variety of local solar times, its dataset could be used to investigate diurnal variation of NO in the MLT region.

Bibliography

Barth, C. A.: Nitric oxide in the lower thermosphere, Planetary and space science, 40, 315–336, 1992.

Barth, C. A., Tobiska, W. K., Siskind, D. E., and Cleary, D. D.: Solar-terrestrial coupling: Low-latitude thermospheric nitric oxide, Geophysical research letters, 15, 92–94, 1988.

Barth, C. A., Bailey, S. M., and Solomon, S. C.: Solar-terrestrial coupling: Solar soft x-rays and thermospheric nitric oxide, Geophysical research letters, 26, 1251–1254, 1999.

Bender, S., Sinnhuber, M., Burrows, J. P., Langowski, M., Funke, B., and Lopez-Puertas, M.: Retrieval of nitric oxide in the mesosphere and lower thermosphere from SCIAMACHY limb spectra, Atmospheric Measurement Techniques, 6, 2521–2531, https://doi.org/{10.5194/amt-6-2521-2013}, 2013.

Bender, S., Sinnhuber, M., von Clarmann, T., Stiller, G., Funke, B., Lopez-Puertas, M., Urban, J., Perot, K., Walker, K. A., and Burrows, J. P.: Comparison of nitric oxide measurements in the mesosphere and lower thermosphere from ACE-FTS, MIPAS, SCIAMACHY, and SMR, Atmospheric Measurement Techniques, 8, 4171–4195, https://doi.org/{10.5194/amt-8-4171-2015}, 2015.

Bernath, P. F., McElroy, C. T., Abrams, M., Boone, C. D., Butler, M., Camy-Peyret, C., Carleer, M., Clerbaux, C., Coheur, P.-F., Colin, R., et al.: Atmospheric chemistry experiment (ACE): mission overview, Geophysical Research Letters, 32, 2005.

Elsasser, W. M.: On the origin of the Earth's magnetic field, Physical Review, 55, 489, 1939.

Eriksson, P.: Microwave radiometric observations of the middle atmosphere: Simulations and inversions, Chalmers University of Technology, 1999.

Eriksson, P., Buehler, S., Davis, C., Emde, C., and Lemke, O.: ARTS, the atmospheric radiative transfer simulator, version 2, Journal of Quantitative Spectroscopy and Radiative Transfer, 112, 1551–1558, 2011.

Eyring, V., Bony, S., Meehl, G. A., Senior, C. A., Stevens, B., Stouffer, R. J., and Taylor, K. E.: Overview of the Coupled Model Intercomparison Project Phase 6 (CMIP6) experimental design and organization, Geoscientific Model Development, 9, 1937–1958, 2016.

Fischer, H., Birk, M., Blom, C., Carli, B., Carlotti, M., Clarmann, T. v., Delbouille, L., Dudhia, A., Ehhalt, D., Endemann, M., et al.: MIPAS: an instrument for atmospheric and climate research, Atmospheric Chemistry and Physics, 8, 2151–2188, 2008.

Fisher, M., O'Neill, A., and Sutton, R.: Rapid descent of mesospheric air into the stratospheric polar vortex, Geophysical research letters, 20, 1267–1270, 1993.

Gérard, J.-C. and Barth, C.: High-latitude nitric oxide in the lower thermosphere, Journal of Geophysical Research, 82, 674–680, 1977.

Gordley, L. L., Hervig, M. E., Fish, C., Russell, J. M., Bailey, S., Cook, J., Hansen, S., Shumway, A., Paxton, G., Deaver, L., et al.: The solar occultation for ice experiment, Journal of Atmospheric and Solar-Terrestrial Physics, 71, 300–315, 2009.

Gray, L. J., Beer, J., Geller, M., Haigh, J. D., Lockwood, M., Matthes, K., Cubasch, U., Fleitmann, D., Harrison, G., Hood, L., et al.: Solar influences on climate, Reviews of Geophysics, 48, 2010.

Hendrickx, K., Megner, L., Gumbel, J., Siskind, D. E., Orsolini, Y. J., Tyssoy, H. N., and Hervig, M.: Observation of 27day solar cycles in the production and mesospheric descent of EPP-produced NO, Journal of Geophysical Research-Space Physics, 120, 8978–8988, https://doi.org/{10.1002/2015JA021441}, 2015.

Konopka, P., Engel, A., Funke, B., Müller, R., Grooß, J.-U., Günther, G., Wetter, T., Stiller, G., von Clarmann, T., Glatthor, N., et al.: Ozone loss driven by nitrogen oxides and triggered by stratospheric warmings can outweigh the effect of halogens, Journal of Geophysical Research: Atmospheres, 112, 2007.

Labitzke, K. and Kunze, M.: On the remarkable Arctic winter in 2008/2009, Journal of Geophysical Research: Atmospheres, 114, 2009.

Lutgens, F. K., Tarbuck, E. J., and Tusa, D.: The atmosphere, Prentice Hall Upper Saddle River, NJ, 2001.

Marsh, D., Solomon, S., and Reynolds, A.: Empirical model of nitric oxide in the lower thermosphere, Journal of Geophysical Research-Space Physics, 109, https://doi.org/{10.1029/2003JA010199}, 2004.

Marsh, D. R. and Russell, J. M.: A tidal explanation for the sunrise/sunset anomaly in HALOE low-latitude nitric oxide observations, Geophysical research letters, 27, 3197–3200, 2000.

McCoy, D.: Why Odin is one eyed, URL `https://norse-mythology.org/gods-and-creatures/the-aesir-gods-and-goddesses/odin/`, 2017.

Menvielle, M. and Berthelier, A.: The K-derived planetary indexes - description and availability, Reviews of Geophysics, 29, 415–432, https://doi.org/{10.1029/91RG00994}, 1991.

Menvielle, M., Iyemori, T., Marchaudon, A., and Nosé, M.: Geomagnetic indices, in: Geomagnetic Observations and Models, pp. 183–228, Springer, 2011.

Minschwaner, K. and Siskind, D.: A New Calculation of Nitrix-Oxide Photolysis in the Stratosphere, Mesosphere, and Lower Thermosphere, Journal of Geophysical Research-Atmospheres, 98, 20 401–20 412, https://doi.org/{10.1029/93JD02007}, 1993.

Murtagh, D., Frisk, U., Merino, F., Ridal, M., Jonsson, A., Stegman, J., Witt, G., Eriksson, P., Jiménez, C., Megie, G., et al.: An overview of the Odin atmospheric mission, Canadian Journal of Physics, 80, 309–319, 2002.

NOAA: F10.7 cm Radio Emissions, URL http://www.swpc.noaa.gov/phenomena/f107-cm-radio-emissions.

NOAA: Aurora Forecast, URL http://services.swpc.noaa.gov/images/aurora-forecast-northern-hemisphere.jpg, a.

NOAA: Aurora Forecast, URL http://services.swpc.noaa.gov/images/aurora-forecast-southern-hemisphere.jpg, b.

Nordh, H., Von Schéele, F., Frisk, U., Ahola, K., Booth, R., Encrenaz, P., Hjalmarson, Å., Kendall, D., Kyrölä, E., Kwok, S., et al.: The Odin orbital observatory, Astronomy & Astrophysics, 402, L21–L25, 2003.

NWRA: NorthWest Research Associates, Inc. Space Weather Services. Geomagnetic Latitude., URL https://spawx.nwra.com/spawx/maps/maplats.html.

Pérot, K., Urban, J., and Murtagh, D. P.: Unusually strong nitric oxide descent in the Arctic middle atmosphere in early 2013 as observed by Odin/SMR, Atmospheric Chemistry and Physics, 14, 8009–8015, https://doi.org/{10.5194/acp-14-8009-2014}, 2014.

Rodgers, C. D.: Retrieval of atmospheric temperature and composition from remote measurements of thermal radiation, Reviews of Geophysics, 14, 609–624, 1976.

SABER: SABER Science, Measurement Approach and Data Product Overview, URL http://slideplayer.com/slide/3231660/11/images/9/LIMB+EMISSION+EXPERIMENT+VIEWING+GEOMETRY+AND+INVERSION+APPROACH.jpg.

Schoeberl, M. R., Lait, L. R., Newman, P. A., and Rosenfield, J. E.: The structure of the polar vortex, Journal of Geophysical Research: Atmospheres, 97, 7859–7882, 1992.

Sheese, P., Strong, K., Gattinger, R., Llewellyn, E., Urban, J., Boone, C., and Smith, A.: Odin observations of Antarctic nighttime NO densities in the mesosphere–lower thermosphere and observations of a lower NO layer, Journal of Geophysical Research: Atmospheres, 118, 7414–7425, 2013.

Sinnhuber, M., Nieder, H., and Wieters, N.: Energetic particle precipitation and the chemistry of the mesosphere/lower thermosphere, Surveys in Geophysics, 33, 1281–1334, 2012.

Siskind, D. E., Barth, C., and Russell, J.: A climatology of nitric oxide in the mesosphere and thermosphere, Advances in Space Research, 21, 1353–1362, 1998.

Smith, K. L., Neely, R., Marsh, D., and Polvani, L. M.: The Specified Chemistry Whole Atmosphere Community Climate Model (SC-WACCM), Journal of Advances in Modeling Earth Systems, 6, 883–901, 2014.

Solomon, S. C., Barth, C. A., and Bailey, S. M.: Auroral production of nitric oxide measured by the SNOE satellite, Geophysical research letters, 26, 1259–1262, 1999.

Strobel, D. F.: Diurnal variation of nitric oxide in the upper atmosphere, Journal of Geophysical Research, 76, 2441–2452, 1971.

Tapping, K. and Detracey, B.: The origin of the 10.7cm flux, Solar Physics, 127, 321–332, https://doi.org/{10.1007/BF00152171}, 1990.

Thebault, E., Finlay, C. C., Beggan, C. D., Alken, P., Aubert, J., Barrois, O., Bertrand, F., Bondar, T., Boness, A., Brocco, L., Canet, E., Chambodut, A., Chulliat, A., Coisson, P., Civet, F., Du, A., Fournier, A., Fratter, I., Gillet, N., Hamilton, B., Hamoudi, M., Hulot, G., Jager, T., Korte, M., Kuang, W., Lalanne, X., Langlais, B., Leger, J.-M., Lesur, V., Lowes, F. J., Macmillan, S., Mandea, M., Manoj, C., Maus, S., Olsen, N., Petrov, V., Ridley, V., Rother, M., Sabaka, T. J., Saturnino, D., Schachtschneider, R., Sirol, O., Tangborn, A., Thomson, A., Toffner-Clausen, L., Vigneron, P., Wardinski, I., and Zvereva, T.: International Geomagnetic Reference Field: the 12th generation, Earth Planets and Space, 67, https://doi.org/{10.1186/s40623-015-0228-9}, 2015.

University of Colorado Boulder: Research, URL `http://lasp.colorado.edu/home/mag/research/`.

Urban, J., Lautié, N., Le Flochmoën, E., Jiménez, C., Eriksson, P., de La Noë, J., Dupuy, E., Ekström, M., El Amraoui, L., Frisk, U., et al.: Odin/SMR limb observations of stratospheric trace gases: Level 2 processing of ClO, N2O, HNO3, and O3, Journal of Geophysical Research: Atmospheres, 110, 2005.

Wallace, J. M. and Hobbs, P. V.: Atmospheric science: an introductory survey, vol. 92, Academic press, 2006.